Representing and Selecting Vibrational Angular Momentum States for Quasiclassical Trajectory Chemical Dynamics Simulations †

ARTICLE *in* THE JOURNAL OF PHYSICAL CHEMISTRY A · NOVEMBER 2007

Impact Factor: 2.69 · DOI: 10.1021/jp073317v · Source: PubMed

3 AUTHORS, INCLUDING:

Upakarasamy Lourderaj
The National Institute of Science Education a…
26 PUBLICATIONS **528** CITATIONS

SEE PROFILE

Emilio Martinez-Nuñez
University of Santiago de Compostela
85 PUBLICATIONS **1,018** CITATIONS

SEE PROFILE

Representing and Selecting Vibrational Angular Momentum States for Quasiclassical Trajectory Chemical Dynamics Simulations†

Upakarasamy Lourderaj,‡ Emilio Martínez-Núñez,§ and William L. Hase*,‡

Department of Chemistry and Biochemistry, Texas Tech University, Lubbock, Texas 79409-1061, and Departamento de Química Física, Universidad de Santiago de Compostela, E-15782, Santiago de Compostela SPAIN

Received: April 30, 2007; In Final Form: July 16, 2007

Linear molecules with degenerate bending modes have states, which may be represented by the quantum numbers N and L. The former gives the total energy for these modes and the latter identifies their vibrational angular momentum j_z. In this work, the classical mechanical analog of the N,L-quantum states is reviewed, and an algorithm is presented for selecting initial conditions for these states in quasiclassical trajectory chemical dynamics simulations. The algorithm is illustrated by choosing initial conditions for the $N = 3$ and $L = 3$ and 1 states of CO_2. Applications of this algorithm are considered for initial conditions without and with zero-point energy (zpe) included in the vibrational angular momentum states and the C−O stretching modes. The O-atom motions in the x,y-plane are determined for these states from classical trajectories in Cartesian coordinates and are compared with the motion predicted by the normal-mode model. They are only in agreement for the $N = L = 3$ state without vibrational angular momentum zpe. For the remaining states, the Cartesian O-atom motions are considerably different from the elliptical motion predicted by the normal-mode model. This arises from bend−stretch coupling, including centrifugal distortion, in the Cartesian trajectories, which results in tubular instead of elliptical motion. Including zpe in the C−O stretch modes introduces considerable complexity into the O-atom motions for the vibrational angular momentum states. The short-time O-atom motions for these trajectories are highly irregular and do not appear to have any identifiable characteristics. However, the O-atom motions for trajectories integrated for substantially longer period of times acquire unique properties. With C−O stretch zpe included, the long-time O-atom motion becomes tubular for trajectories integrated to ∼14 ps for the $L = 3$ states and to ∼44 ps for the $L = 1$ states.

I. Introduction

Classical trajectory simulations are widely used to study the atomic-level dynamics of molecular collisions.[1] If quantum effects, such as tunneling,[2] interferences,[3] and the unphysical flow of zero-point energy,[4,5] do not dominate a chemical process, then numerous studies[6] indicate that classical mechanics gives a very good representation of the system's chemical dynamics. The agreement between experiment and simulation is often enhanced if initial conditions are chosen for the reactants to represent their quantum vibrational and rotational states.[1] These initial conditions are called quasiclassical and are selected for an ensemble of trajectories with proper weighting of coordinate and momenta phase space points. Such quasiclassical trajectory simulations have included studies of gas-phase, gas−surface, and condensed-phase chemical dynamics. Illustrative examples of the accuracy of the simulations include calculations of intramolecular vibrational energy relaxation times,[7] bimolecular cross sections,[8] unimolecular product energy partitioning,[9] gas−surface collisional energy transfer,[10] and photodissociation dynamics.[11]

In recent experiments,[12,13] NO_2^+ + rare-gas and NO_2^+ + C_2H_2 collisions have been studied with NO_2^+ prepared in specific vibrational angular momentum states. These states are present in linear molecules and arise from a pair of degenerate linear bending motions.[14−17] Previously, Schatz[18] and Child[19] described the semiclassical states for these degenerate bends. In this article an approach is described for selecting quasiclassical initial conditions for vibrational angular momentum states of polyatomic molecules, and contact is made with the previous semiclassical work.[18,19] The quantum mechanical description of the vibrational angular momentum states, and their semiclassical and classical analogues, are described in Section II. Selecting quasiclassical initial conditions for the normal modes of the molecule, including vibrational angular momentum states, is described in Section III. Illustrations of choosing quasiclassical initial conditions for the stretch and degenerate bend modes of CO_2 are described in Section IV. A summary is given in Section V.

II. Vibrational Angular Momentum States

A. Quantum Mechanical Representation. For the harmonic oscillator and separable rotation−vibration model, the total energy for a linear molecule's pair of normal-mode degenerate bends is given by eq 1,[15−17]

$$E = (n_a + 1/2)h\nu + (n_b + 1/2)h\nu = (N + 1)h\nu \qquad (1)$$

where the n's are the bends' vibrational quantum numbers, and $N = n_a + n_b$. Each value of N is associated with $N + 1$ degenerate energy levels and wave functions $\Psi(n_a,n_b)$ corre-

† Part of the special issue "Robert E. Wyatt Festschrift".

* To whom correspondence should be addressed. E-mail: bill.hase@ttu.edu.
‡ Texas Tech University.
§ Universidad de Santiago de Compostela.

10.1021/jp073317v CCC: $37.00
Published on Web 09/08/2007

sponding to different possible combinations of n_a and n_b. The wave functions are $\Psi(2, 0)$, $\Psi(1, 1)$, and $\Psi(0, 2)$ for the $N = 2$ degenerate vibrational levels. Classically, if both modes are excited, as for the $\Psi(1, 1)$ state, then the bending vibrations give rise to vibrational angular momentum j_z about the internuclear z-axis.[14−17]

Though the wave functions $\Psi(n_a,n_b)$ provide an adequate description of the bending vibrations, any proper linear combination of the wave functions for the degenerate levels also furnishes an adequate representation. The vibrational angular momentum is not quantized by the $\Psi(n_a,n_b)$ states, and it is of particular interest to choose a linear combination that satisfies this quantization. The exact form of this linear combination is described elsewhere.[15−17] For the current presentation it is only necessary to know that these wave functions are eigenfunctions of both the vibrational Hamiltonian and vibrational angular momentum operators, giving rise to $N + 1$ degenerate energy levels with $E = (N+1)h\nu$. The vibrational angular momenta for the states are $j_z = L\hbar$, with $L = N, N-2, \ldots -(N-2), -N$.

B. Semiclassical Mechanical Representation. Child[19] has described degenerate harmonic oscillators in terms of semiclassical action-angle variables and provided the relationship between the oscillator's semiclassical and quantum mechanical descriptions. The degenerate bend's classical Hamiltonian is given by eq 2,

$$H = (P_a^2 + P_b^2)/2 + \lambda(Q_a^2 + Q_b^2)/2 \quad (2)$$

where λ, the bend's normal-mode eigenvalue, equals $4\pi^2\nu^2$, and P_a and Q_a are the normal mode's momentum and co-ordinate, respectively. The actions are shown in eqs 3 and 4,

$$I = (N + 1)\hbar \quad (3)$$

$$j_z = L\hbar \quad (4)$$

and their associated angle variables, which range between 0 and 2π, are α_I and α_j, respectively. The energy for the degenerate bends is $E = I\omega$, where $\omega = 2\pi\nu$. As discussed in the next section, the motion associated with the 2-dimensional (2D) Hamiltonian of the degenerate bends is elliptical, where α_I describes the motion around the ellipse, and α_j defines the orientation of the major-axis of the ellipse in the molecular plane. The transformations between these action-angle variables and the normal-mode coordinates and momenta are given by eqs 5a−d.

$$Q_a = [(I + j_z)/\omega]^{1/2} \cos(\alpha_I + \alpha_j) \quad (5a)$$

$$Q_b = [(I - j_z)/\omega]^{1/2} \cos(\alpha_I - \alpha_j) \quad (5b)$$

$$P_a = -[(I + j_z)/\omega]^{1/2} \sin(\alpha_I + \alpha_j) \quad (5c)$$

$$Q_a = -[(I + j_z)/\omega]^{1/2} \sin(\alpha_I - \alpha_j) \quad (5d)$$

The above equations suffice for choosing initial conditions for the degenerate bend's 2D Hamiltonian. The energy and angular momentum for the quantum state are given by the actions I and j_z, and the angles α_I and α_j are chosen randomly between 0 and 2π. However, for the problem considered here, initial conditions are chosen for all $(3n - 5)$ degrees of freedom of the molecular Hamiltonian. For this multidimensional sampling, it is convenient to choose initial conditions using normal-mode coordinates and momenta. The classical normal-mode motion associated with the degenerate bends is described in the next section.

C. Classical Mechanical Representation. Depending on the relative phase of the two degenerate bend modes, the classical motion for their zero-point energy (zpe) level may contain vibrational angular momentum. In the following, classical representations of the degenerate linear bends are described with and without zpe. The condition considered is the one in which each of the bend modes contains the same energy.

1. Vibrational Angular Momentum zpe Not Included. The energy in each degenerate bend is $Nh\nu/2$, if each of the bends has the same energy and if zpe is not included. The value of L is set by the difference in the phase of the two bending motions. The classical energy for each bend mode, as denoted by that for mode a, is given by eq 6,

$$E_a = Nh\nu/2 = (P_a^2 + \lambda Q_a^2)/2 \quad (6)$$

with maximum P_a and Q_a of $P^\circ = (2E_a)^{1/2}$ and $Q^\circ = (2E_a/\lambda)^{1/2}$. One co-ordinate moves in the x,z-plane and the other in the y,z-plane, and their time dependencies may be written by eqs 7a−b,

$$Q_{x,z}(t) = Q^\circ \cos(2\pi\nu t) \quad (7a)$$

$$Q_{y,z}(t) = Q^\circ \cos(2\pi\nu t - \varphi) \quad (7b)$$

where φ is the difference in the phase of the two bends. For the x,z-bend, at $t = 0$ all of the energy is potential. The normal-mode momenta are the time derivatives of these coordinates (i.e.. eqs 8a−b).

$$P_{x,z}(t) = -P^\circ \sin(2\pi\nu t) \quad (8a)$$

$$P_{y,z}(t) = -P^\circ \sin(2\pi\nu t - \varphi) \quad (8b)$$

The vibrational angular momentum is given by eq 9.

$$j_z = Q_{x,z}P_{y,z} - Q_{y,z}P_{x,z} \quad (9)$$

The maximum value for the vibrational angular momentum (i.e., $j_z = N\hbar$) occurs when the two modes are 90° out-of-phase (i.e., $\varphi = 90°$). For this case, when the x,z-mode is at its classical turning point with all of its energy in potential, the y,z-mode is at its potential minimum with all of its energy in kinetic. This condition may be used to determine the vibrational angular momentum, which is $j_z = Q^\circ P^\circ = N\hbar$. For the $L = -N$ state, the sign of P° is reversed. The value of φ for the remaining L states is found by setting the x,z-mode at its classical turning point, as above, with all of its energy in potential and choosing a value of $P_{y,z}$, for motion in the y,z-plane, so that the vibrational angular momentum equals $L\hbar$. Thus, $j_z = Q^\circ P_{y,z} = L\hbar$ with $P_{y,z}/P^\circ = L/N$. From eqs 8a and 8b, the phase difference between the motions in the x,z- and y,z-planes is then $\varphi = \sin^{-1}(L/N)$, so that the vibrational angular momentum becomes eq 10.

$$j_z = Q^\circ P^\circ \sin\varphi = N\hbar \sin\varphi \quad (10)$$

The initial value for $Q_{y,z}$, for motion in the y,z-plane, is $[2E_a - (P^\circ \sin\varphi)^2]/2$. For $L = 0$, $\varphi = 0$ and the two modes vibrate in-phase. When the x,z-mode is at its classical turning point with $Q_{x,z} = Q^\circ$, the coordinate for the $Q_{y,z}$ mode is also Q°.

The rotational energy associated with the vibrational angular momentum is given by eq 11,

$$E_{rot} = j_z^2/2I_L \quad (11)$$

where $j_z = L\hbar$, and I_L is the moment of inertia for the L state. As described above, for the $L = 0$ state, the two bend modes vibrate in-phase with their energy oscillating between all-potential and all-kinetic with a period of $1/(2\upsilon)$.[18] There is no rotational angular momentum, and $E_{rot} = 0$. For the $L = N$ state, I_L is a constant and does not change during the vibrational motion. For the mass-weighted normal-mode coordinates, this I_L is given by $I_L = (Q^\circ)^2$. This is seen by replacing φ in eq 7b by 90°, so that $Q_{y,z}(t) = Q^\circ \sin(2\pi\upsilon t)$. The mass-weighted radius-squared for the vibrational angular momentum motion is then $[Q_{x,z}(t)^2 + Q_{y,z}(t)^2] = (Q^\circ)^2$. Because $j_z = Q^\circ P^\circ$ for the $L = N$ state, E_{rot} is $(P^\circ)^2/2 = E_a$. Thus, one-half of the total energy E for the two bending modes is rotational, and the other half is the potential energy of the fixed radius rotation.

For the remaining L states, I_L is not a constant and is given by eq 12.

$$I_L(t) = Q_{x,z}(t)^2 + Q_{y,z}(t)^2 \tag{12}$$

Thus, the rotational energy of the degenerate bends changes with time. The average value for $I_L(t)$ may be determined by inserting the expressions in eqs 7a and 7b for $Q_{x,z}(t)$ and $Q_{y,z}(t)$ into eq 12 and averaging over one vibrational period (i.e., eq 13).

$$\langle I_L(t)\rangle = (Q^\circ)^2[\int_0^{\nu^{-1}} \cos^2(2\pi\nu t)\, dt + \int_0^{\nu^{-1}} \cos^2(2\pi\nu t + \varphi)\, dt]/\nu^{-1} \tag{13}$$

It is straightforward to show that the integrals in brackets is equal to υ^{-1}, so that $<I_L(t)> = (Q^\circ)^2$. Thus, for the vibrational angular momentum states with $L \neq |N|$, the average rotational energy of the degenerate bend motions is given by eq 14.

$$<E_{rot}> = \sin^2\varphi (N\hbar)^2/2(Q^\circ)^2 = (L/N)^2\, E/2 \tag{14}$$

where E is the total energy. This expression also holds for the $L = |N|$ states with $\varphi = 90°$. However, as described above for these states, E_{rot} is constant during the bending vibration, and an average is not required.

2. Vibrational Angular Momentum zpe Included. With zpe included, the total classical energy for the two bend modes is $E = (N + 1)h\upsilon$. The energy of the zpe level is $h\upsilon$ and, depending on the relative phase of the two modes, this level can have vibrational angular momentum j_z. If the two modes are in-phase then $j_z = 0$, but $j_z = \hbar$ if they are 90° out-of-phase. As discussed above, quantum mechanically, the zpe level does not have vibrational angular momentum. Nonzero values of j_z are associated with excited bend levels, with $j_z = L\hbar$, $L = N, N-2, \ldots, -(N-2), -N$, and $N = n_a + n_b$. The vibrational angular momentum is given by eq 15.

$$j_z = (N + 1)\hbar \sin\varphi \tag{15}$$

With zpe included, the maximum value for the relative phase (φ) between the two bend modes is less than 90° for the $L = |N|$ states, because setting $\varphi = 90°$ results in $j_z = (N + 1)\hbar$. The selection of φ for different L-states, including $L = |N|$, follows the presentation in the previous section. The x,z-mode is placed at its classical turning point with $Q_{x,z} = Q^\circ$ and $P_{x,z} = 0$. A value for the momentum ($P_{y,z}$) for the other mode is chosen so that the vibrational angular momentum equals $L\hbar$. The resulting value of $P_{y,z}$ is $P^\circ L/(N + 1)$, so that $j_z = Q^\circ P_{y,z} = Q^\circ P^\circ L/(N + 1) = L\hbar$. The phase difference between the motions in the x,z- and y,z-planes is then $\varphi = \sin^{-1}[L/(N + 1)]$. For the $L = N$ state, $\varphi \neq 90°$ and $\varphi = \sin^{-1}[N/(N + 1)]$.

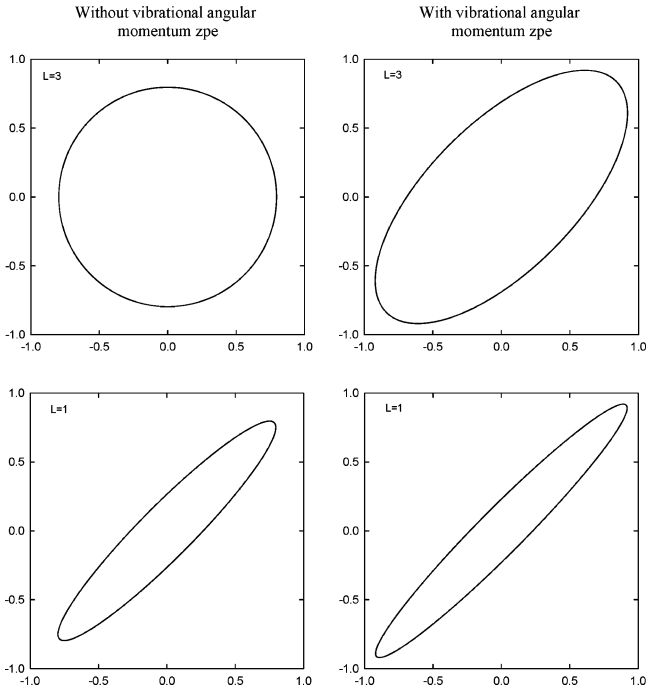

Figure 1. Plots of $Q_{x,z}(t)$ versus $Q_{y,z}(t)$ for CO_2, with CO_2 prepared in vibrational angular momentum states with $N = 3$ and $L = 3$ and 1. The motion is determined from eqs 3a and 3b of the normal-mode model. Plots are given for states with and without vibrational angular momentum zpe. The normal-mode coordinates are in units of $(amu)^{1/2}$ Å.

Because the two bends are not 90° out-of-phase for the $L = N$ state, the motion associated with the vibrational angular momentum for this state is not circular but is elliptical, as are the other L-states. Thus, the rotational energy for each L-state is an average for one vibrational period and is found from the average moment of inertia (i.e., $<I_L(t)>$ in eq 13). The expression for $<E_{rot}>$ is given by eq 16 and is similar to eq 14.

$$<E_{rot}> = [L/(N + 1)]^2 E/2 \tag{16}$$

The total energy E is $(N + 1)h\upsilon$.

3. Classical Motion. It is of interest to consider the classical dynamics in Cartesian coordinates for different vibrational angular momentum states of the above normal-mode model, and Figure 1 gives plots of $Q_{x,z}(t)$ versus $Q_{y,z}(t)$ (i.e. Eqs 7a and 7b, for CO_2). The vibrational frequency for the degenerate linear bend is 667 cm^{-1}. The phase angle φ is 90° for the $L = N = 3$ state, with no zpe, and the motion is circular. The remaining three states have a phase angle less than 90°, and their motion is elliptical. Because the normal-mode model has a linear transformation between normal-mode coordinates and Cartesian displacement coordinates,[20] these plots also describe the motion of each of the O-atoms in the x,y-plane. For the one state it is circular, but it is elliptical for the other three.[14,15,17]

For the motions in Figure 1, each of the degenerate bends contains one-half of the total energy, and this fixes the major-axis at 45° from the x- and y-axes of the plane for their elliptical motion. Random orientation of the major-axis in this plane (α_j for the semiclassical description in Section II.B) is obtained by randomly rotating the molecule (see the next section).

The motions in Figure 1 are initiated with the x,z-mode at its classical turning point, and $Q_{y,z}$ is set by the phase angle φ (eq 7b). For this 2D model, the resulting motion is independent of the initial value for $Q_{x,z}$ and will lie on the circle/ellipse in

Figure 1. However, as described in the following, the interest here is in including vibrational angular momentum states as part of the $(3n - 5)$ vibrational degrees of freedom of a linear molecule. All of these degrees of freedom are coupled, and the classical motion (i.e., trajectory) for the molecule will depend on the initial value for $Q_{x,z}$. Thus, it is necessary to select the initial value for $Q_{x,z}$ randomly, and this is done by choosing a random phase $2\pi R$ for this mode so that $Q_{x,z} = Q^\circ \cos(2\pi R)$.[1] The angle for mode $Q_{y,z}$ (eq 7b) is then $2\pi R - \varphi$. Here R is a fresh random number between 0 and 1.

III. Selecting Initial Cartesian Coordinates and Momenta for Vibrational Angular Momentum States

A. Algorithm Without Vibrational Angular Momentum. Initial Cartesian coordinates and momenta for a polyatomic molecule with degenerate bend motions, and vibrational angular momentum states, may be selected by a minor modification of an algorithm used to select quasiclassical initial conditions for polyatomic molecules. This algorithm, described in detail previously,[1] is briefly reviewed in the following procedure: (1) The first step is to determine the molecule's normal-mode frequencies ($\omega = 2\pi\nu$) and normal-mode eigenvector (**L**) by diagonalizing its mass-weighted Cartesian force constant matrix.[20] (2) For a mode-specific simulation, the quantum numbers (n_i) for the normal-modes are either specified or chosen randomly from their Boltzmann distributions. The total vibrational energy is $E_\nu^\circ = \sum(n_i + 1/2)h\nu_i$. (3) The normal-mode energies are transformed to normal-mode coordinates (Q_i) and momenta (P_i) by choosing a random phase for each normal-mode. (4) The normal mode **Q** and **P** are transformed to Cartesian coordinates **q** and momenta **p** for N atoms using the normal-mode eigenvector **L**.[20] (5) Because normal modes are approximate for finite displacements,[20] a spurious angular momentum ($\mathbf{j}_s$) may arise following this transformation.[20,21] This spurious angular momentum is calculated. (6) The rotational angular momentum and its components are added. A nonlinear molecule is treated as a symmetric top with rotational quantum numbers J and K. If J and K are specified, the components of the angular momentum are found from eqs 17a−d,

$$j = \sqrt{J(J+1)}\hbar \tag{17a}$$

$$j_z = K\hbar \tag{17b}$$

$$j_x = (j^2 - j_z^2)^{1/2} \sin(2\pi R) \tag{17c}$$

$$j_y = (j^2 - j_z^2)^{1/2} \cos(2\pi R) \tag{17d}$$

where R is a random number. For thermal experiments, it is usually accurate to sample j and j_z from their classical Boltzmann distributions,[22] with j_x and j_y, found from eqs 17c and 17d. The components j_x, j_y, and j_z, form the desired angular momentum vector $\mathbf{j}^\circ$. Equilibrium coordinates for linear polyatomic molecules are placed on the z-axis with its rotational angular momentum (j) initially along the x- or y-axis; e.g. $j = j_x$. (7) The angular momentum $\mathbf{j}^\circ$ is added to the molecule by forming the vector shown in eq 19,

$$\mathbf{j} = \mathbf{j}^\circ - \mathbf{j}_s \tag{18}$$

and adding the rotational velocity $\omega \times \mathbf{r}_i$ to each of the atoms, where

$$\omega = I^{-1}\mathbf{j} \tag{19}$$

and I^{-1} is the inverse of the inertia tensor.[23] (8) The rotational energy (E°_r) is calculated from angular momentum components and the principal moments of inertia. The total energy of the molecule is the sum of its vibrational and rotational energies, that is, $E^\circ = E^\circ_\nu + E^\circ_r$. (9) The actual internal energy (E) for the Cartesian coordinates and momenta chosen from the above steps is calculated using the correct Hamiltonian and compared with the intended energy (E°). If they do not agree within some acceptance criterion (i.e., 0.1% in VENUS[24]), the Cartesian coordinates and momenta are scaled assuming the energy is quadratic in momenta and coordinate displacement from equilibrium (i.e., eq 2.27 in ref 1). Any spurious center-of-mass translational energy is subtracted from the molecule, and the procedure loops back to step five where the spurious angular momentum is calculated. If the energies do agree within the acceptance criterion, the molecule is randomly rotated about its center-of-mass in the x,y,z-frame.

B. Algorithm with Vibrational Angular Momentum. Selecting initial conditions for a specific vibrational angular momentum state of a linear polyatomic molecule requires choosing Cartesian coordinates and momenta for the molecule that correspond to its vibrational angular momentum quantum numbers N and L, as well as its vibrational and external rotation quantum numbers. This is accomplished by the following minor modifications of the above algorithm (1) In step 2 of the above algorithm, the quantum numbers for the two degenerate bends (n_a and n_b) are equated. If zpe is not included, energy ($E = Nh\nu/2$) is assigned to each of the bend modes, where $N = n_a + n_b$ and ν is the bend frequency. If zpe is included, $E = (N + 1)h\nu/2$ is assigned to each of the bend modes. (2) To assign the quantum number L to the degenerate bends, the normal-mode coordinates and momenta for the two bends are not chosen randomly as described in step 3 above. Instead, they are chosen with the proper relationship as described in Sections II.B and II.C, that is,

$$Q_a = Q^\circ \cos(2\pi \mathrm{R}) \tag{20a}$$

$$P_a = -P^\circ \sin(2\pi \mathrm{R}) \tag{20b}$$

$$Q_b = Q^\circ \cos(2\pi R - \varphi) \tag{20c}$$

$$P_b = -P^\circ \sin(2\pi R - \varphi) \tag{20d}$$

where $Q^\circ = (2E/\lambda)^{1/2}$, $P^\circ = (2E)^{1/2}$, and $\lambda = 4\pi^2\nu^2$. If zpe is not included, then $\sin\varphi = L/N$. With zpe included, $\sin\varphi = L/(N + 1)$. The R term is a random number between 0 and 1. (3) With the equilibrium coordinates for the linear molecule placed on the z-axis, the above normal-mode momenta and coordinates for the two degenerate bends add angular momentum $j_z = L\hbar$ about the z-axis. The total angular momentum added to the molecule $\mathbf{j}^\circ$ is then a vector sum of the rotational angular momentum j_x and the vibrational angular momentum j_z. The vibrational angular momentum j_z is properly added by the phase relationship between the two degenerate bend modes, and eqs 18 and 19 in step seven of the above algorithm add j_x. After the Cartesian coordinates and momenta are scaled, eqs 18−20 ensure the molecule contains both the correct rotational and the vibrational angular momenta.

IV. Illustrations of Choosing Initial Conditions for Vibrational Angular Momentum States

The algorithm described above, for selecting vibrational angular momentum states as part of quasiclassical sampling of

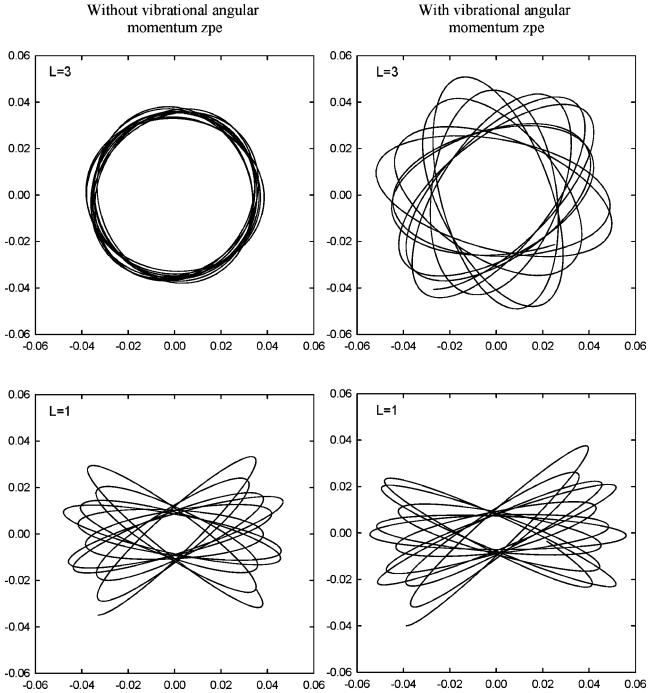

Figure 2. Plots of motion in the *x*,*y*-plane for an O-atom of CO_2, with CO_2 prepared in vibrational angular momentum states with $N = 3$ and $L = 3$ and 1. Zero-point energy is not included in the CO_2 stretch modes. Plots are given for states with and without vibrational angular momentum zpe. Initial conditions are chosen for the trajectories including the rectilinear transformation of step 4 in Section III.A. The trajectories are integrated for 0.5 ps. The Cartesian coordinates are in units of angstroms.

vibrational and rotational energy levels, has been implemented in the general classical trajectory chemical dynamics computer program VENUS.[24] The algorithm is applicable to any vibrational angular momentum state specified by the quantum numbers N and L. In the following, the application of this algorithm is illustrated by selecting vibrational angular momentum states for CO_2 with $N = 3$ and $L = 3$ and 1. Vibrational angular momentum j_z is added to the molecule, with no external rotational angular momentum. Applications of this algorithm are compared by selecting initial conditions with and without zpe in both the vibrational angular momentum states and the symmetric and asymmetric stretch modes. A harmonic CO_2 potential described previously,[25] with stretch and bend force constants of 15.050 mdyn/Å and 0.784 mdyn Å/rad^2, respectively, and an equilibrium C−O bond length of 1.170 Å, was used for these applications.

A. Initial Conditions with no Stretch zpe. Figure 2 gives plots of the O-atom motion in the *x*,*y*-plane for trajectories calculated for 0.5 ps with the above potential energy function and for the $N = 3$ state with $L = 3$ and 1. This integration time is on the order of magnitude of the time it takes for two reactants to collide in a trajectory simulation, given their initial separation. The initial conditions for the trajectories in Figure 2 have no zpe in the CO_2 stretch modes. Without vibrational angular momentum zpe, the motion of the O-atom for the $L = N = 3$ state is nearly circular and is similar to that for the normal-mode model in Figure 1. For the $L = 1$ state without vibrational angular momentum zpe and for the $L = 3$ and 1 states with vibrational angular momentum zpe, the phase angle is less than 90°, and the motion of an O-atom is that of a rotating ellipse and not a "fixed elliptical", as found from the normal-mode model.

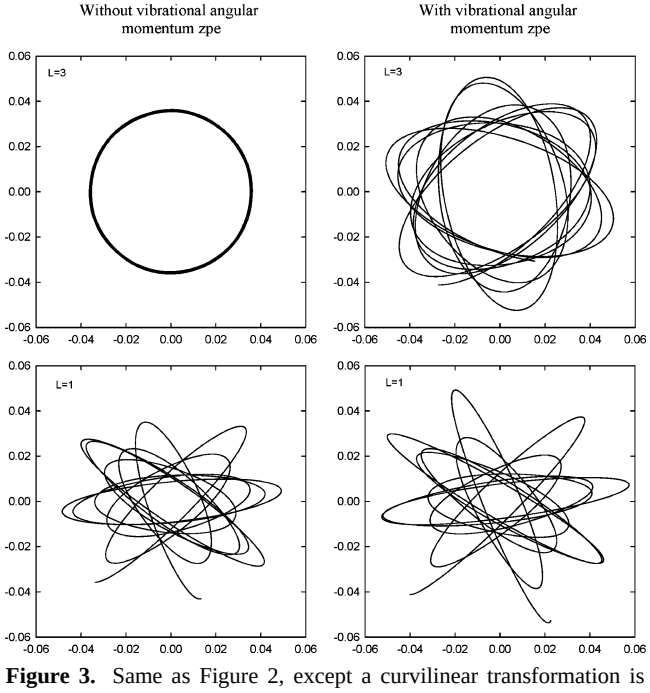

Figure 3. Same as Figure 2, except a curvilinear transformation is used for step 4 in Section III.A.

There are several possible origins of the small fluctuations away from "exact" circular motion for the $L = N = 3$ state without vibrational angular momentum zpe. Centrifugal distortion, which occurs as a result of the vibrational angular momentum, elongates the C−O bonds. This would increase the moment of inertia for a fixed bend angle and cause a change in the bend angle to maintain the constant vibrational angular momentum. Also, as pointed out in much earlier work,[26] even if the potential energy function is harmonic in internal coordinates, as is the case here, there are coupling terms in the Hamiltonian. Such couplings between the bends and the stretches may affect the circular motion. In addition, the rectilinear transformation,[27] in step four of Section III.A, causes a small extension of ∼0.007 Å for each C−O bond, which introduces a small vibrational motion in each bond and perturbs the circular motion.

To assess the importance of the latter effect, a curvilinear transformation from normal mode to Cartesian coordinates was performed, which changes the bend angle without disturbing the C−O bond lengths. The resulting O-atom motion for the N and L states without and with vibrational angular momentum zpe is shown in Figure 3. Comparing Figures 2 and 3 shows that the curvilinear transformation results in a circular type O-atom motion with somewhat weaker perturbations than those found for the rectilinear transformation, but the perturbations remain. Apparently, centrifugal distortion and/or bend−stretch couplings affect the motion of the $L = N = 3$ state without vibrational angular momentum zpe. The curvilinear initial conditions for the $L = N = 3$ state give an O-atom motion comprised of C−O bond lengths that vary from 1.165 to 1.177 Å and a O−C−O angle that varies between 166.1 and 168.2°. For the normal-mode model, these coordinates are fixed at 1.170 Å and 167.15°. As discussed below, using a high force constant for the C−O bond stretch to approximately "fix" the bond at its equilibrium value and eliminate centrifugal distortion and bend−stretch coupling results in a circular plot for the curvilinear model.

There are significant differences between the O-atom motion, for the elliptical states, given by the normal-mode model in

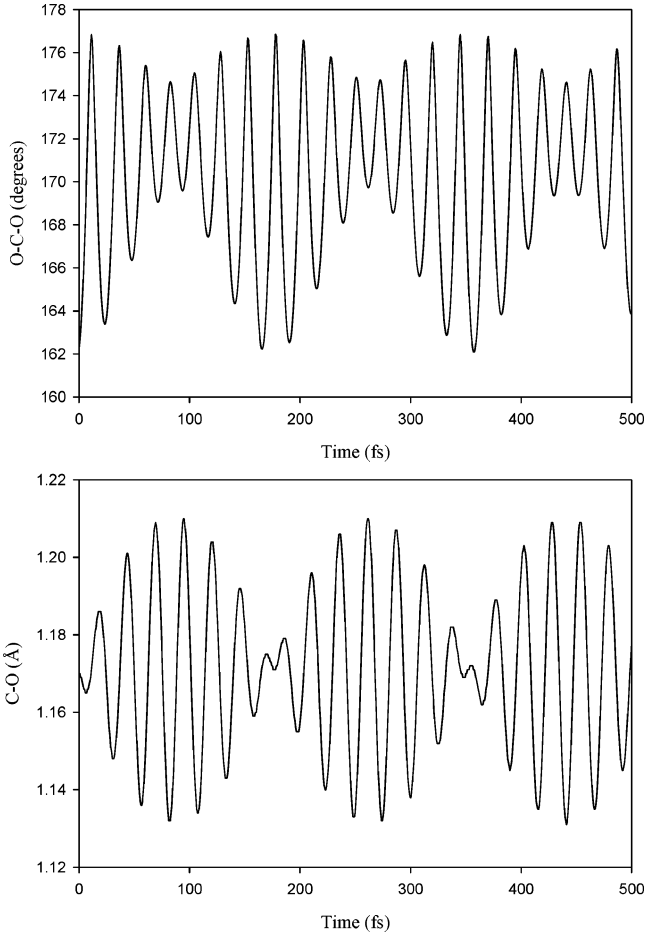

Figure 4. Plot of the O−C−O angle and C−O bond length vs time for the $N = 3$, $L = 1$ trajectory in Figure 3, without vibrational angular momentum.

Figure 1, and the actual Cartesian dynamics in Figures 2 and 3. For these states the O−C−O angle is not fixed, and centrifugal distortion, which is not allowed in the normal-mode model, is an important contributor to the Cartesian dynamics. The angular momentum about the *z*-axis (i.e., j_z) is a constant of the motion and is related to the angular velocity ω_z via $j_z = I_z\omega_z$. As the O−C−O angle changes, I_z changes, which causes ω_z to decrease or increase. These changes in ω_z will perturb the C−O bond lengths. In particular, as the angle increases, approaching 180°, I_z becomes quite small and results in a large angular velocity. This is expected to promote extension of the C−O bonds. Figure 4 gives plots of the O−C−O angle and the C−O bond length versus time for the $N = 3$, $L = 1$ state without vibrational angular momentum zpe and for the curvilinear transformation. There is a regular "beat" between the bend angle and the bond length, which affects the O-atom motion and gives the rotating elliptical motion for the actual Cartesian dynamics. The C−O bond length changes between 1.131 and 1.210 Å.

Changes in the C−O bond length can be constrained by using an artificially high force constant for the C−O bond stretch. Figure 5 shows the O-atom motion for the same states and conditions as in Figure 3, except the C−O stretch force constant has been increased by a factor of 1,000. This results in a nearly exact circular motion for the $L = N = 3$ state without vibrational angular momentum zpe and motion for the other states, which is no longer that of a rotating ellipse and begins to approach that of a fixed ellipse. However, distortions in the elliptical

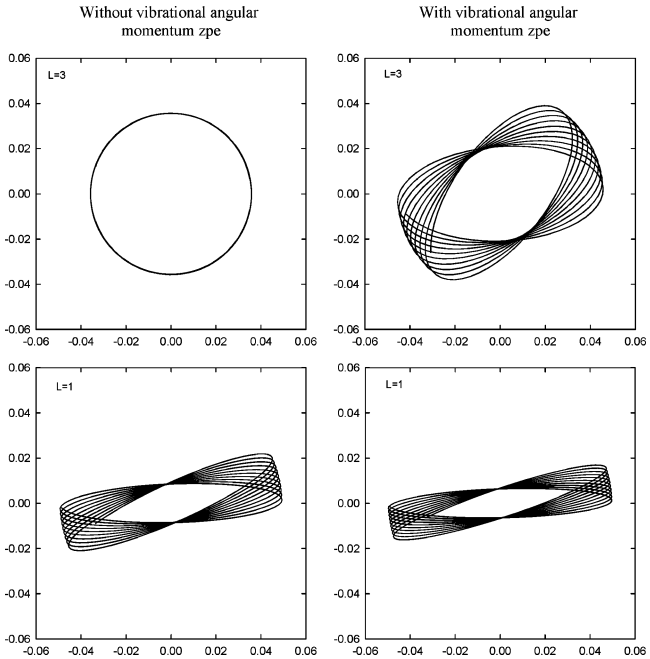

Figure 5. Same as Figure 3, except a C−O stretch force constant 1,000 times larger than the 15.050 mdyn/Å value for the potential function is used.

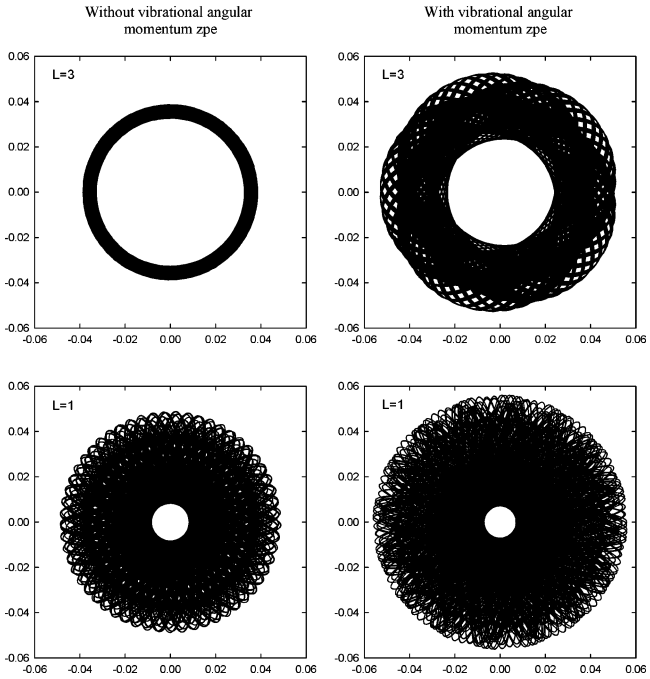

Figure 6. Same as Figure 2, except the trajectory integration time is 20 ps.

motion remain as a result of small changes in the C−O bond lengths, which vary between 1.1701 and 1.1703 Å.

The trajectories in Figure 2 were calculated for 0.5 ps, which, as discussed above, is a representative time required for two reactants to collide in a bimolecular simulations. To obtain a picture of the long-time O-atom motions for these trajectories, they were integrated for 20 ps, and the results are shown in Figure 6. The motion for the $L = 3$ state, without vibrational angular momentum zpe, is similar to the short-time result. However, for the other three states, the short-time trajectories do not identify the long-time O-atom motions. The motion for the $L = 3$ state with vibrational angular momentum zpe has a tubular shape. For the $L = 1$ states, there is an inner oval region

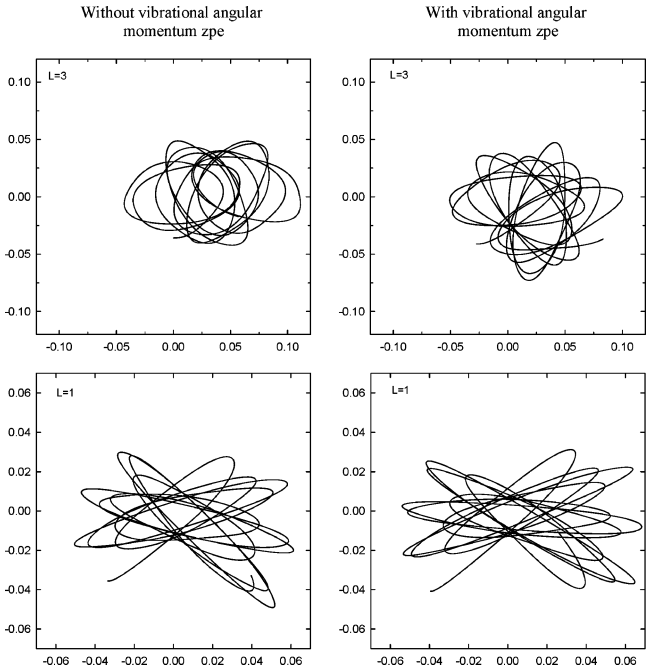

Figure 7. Same as Figure 2, except zpe is included in the stretch modes. These are representative trajectories for the vibrational angular momentum states (see text). The motion is plotted for 0.5 ps.

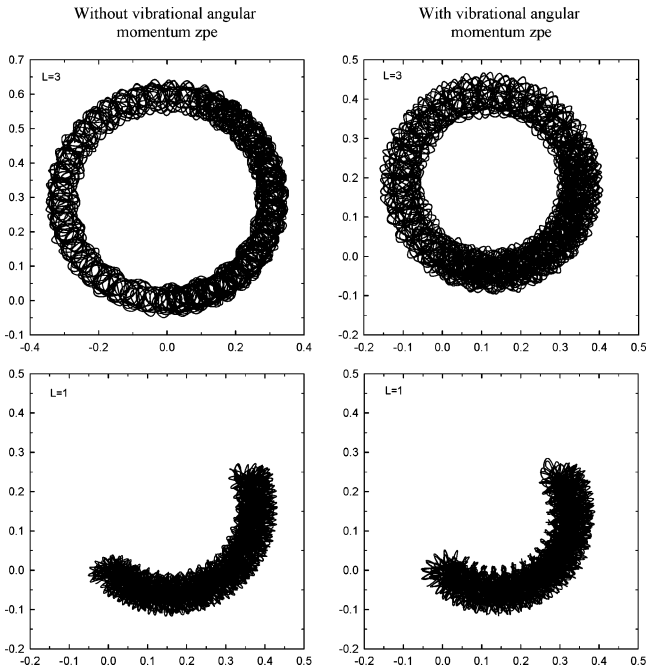

Figure 8. Same as Figure 7, except the trajectory motion is plotted for 20 ps.

about the *x*,*y*-axis origin that is not accessible to the trajectories. This region is larger for the trajectory without vibrational angular momentum.

B. Initial Conditions with Stretch zpe. Adding zpe to the C−O bonds affects the atomic-level dynamics for the vibrational angular momentum states. In Figures 7 and 8, the O-atom motion for representative trajectories of the vibrational angular momentum states, with zpe in the stretch modes, is plotted for different periods of time. Figure 7 depicts the motion for 0.5 ps, which is on the order of magnitude of the time it takes for two reactants to collide in a trajectory simulation, given their initial separation. For the short-time dynamics in Figure 7, the

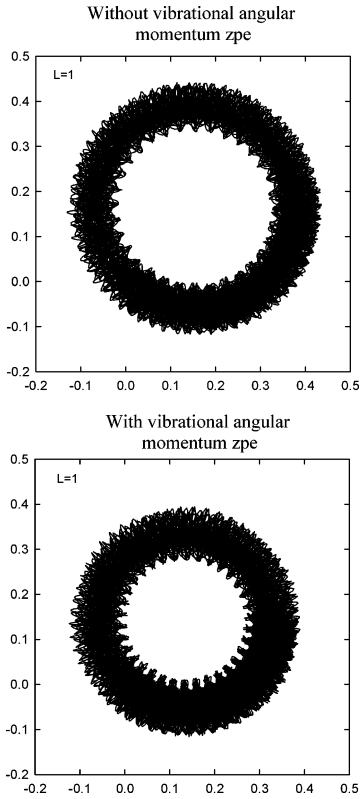

Figure 9. Plots of the O-atom motions, for the $L = 1$ trajectories in Figure 8, for 60 ps.

O-atom motions appear highly irregular[28] and is quite different from those in Figures 1−3.

To study the longer-time motions of individual trajectories for the vibrational angular momentum states, 10 trajectories of 20 ps in length were calculated for each of these states. The long-time motions are significantly different from the short-time motions, and the 10 trajectories for each of the vibrational angular momentum states have qualitatively similar motions. Furthermore, the trajectories with and without vibrational angular momentum zpe, for either the $L = 1$ or 3 state, are similar if they have the same random phases for the C−O stretch modes. For both of the $L = 3$ states, the motion is tubular, as shown in Figure 8. The motions of the 10 trajectories for each state differ in the diameter of the tube and the size of the inner region in which the trajectory does not move. The two trajectories plotted for the $L = 1$ states are representative of the 20 ps O-atom motions for these states. However, as shown in Figure 9, if these trajectories are integrated for 60 ps their overall motions are similar to those for the $L = 3$ states. The requirement of a longer integration time for the $L = 1$ states, to obtain the tubular motion found for the $L = 3$ states, is related to the different angular velocities for these two states, as shown in the following.

An important question, for the states with C−O stretch zpe, is whether the vibrational angular momentum j_z is primarily about the O−C−O internuclear axis. Plotted in Figure 10 are graphs of the angle χ between the *z*-axis and the O−O internuclear axis versus time. The plots are very similar for trajectories with and without vibrational angular momentum zpe if they have the same random phases in the C−O stretch modes, and the plots are only given for the trajectories without vibrational angular momentum zpe. Plots for 10 trajectories are included in each graph. An important observation from the plots is that χ is small and less than 5° for the approximate time of 0.5 ps or less that it takes for two bimolecular reactants to collide

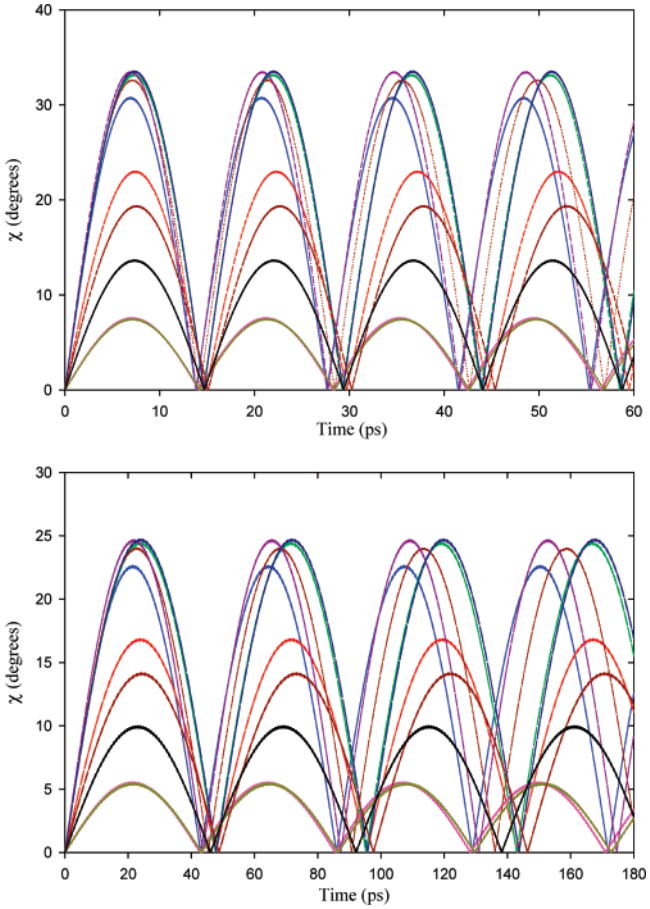

Figure 10. Plots versus time of the angle (χ) between the z-axis and the O−O internuclear axis, for trajectories calculated for the $L = 1$ and 3 states without vibrational angular momentum zpe. Plots for 10 trajectories are included in each graph. The upper graph is for $L = 3$ and the lower one for $L = 1$.

in a chemical dynamics simulation. Thus, the vibrational angular momentum is primarily about the internuclear axis as the collision occurs. For longer times, the χ-angle appears to oscillate periodically with a period of 13.8−15.1 ps for the $L = 3$ states and 42.9−48.8 ps for the $L = 1$ states. For 10 trajectories with vibrational angular momentum zpe included, these periods are 14.2−16.0 ps and 43.2−50.2 ps for the $L = 3$ and 1 states, respectively. The period is approximately 3 times longer for the $L = 1$ state as compared to the $L = 3$ state, which is consistent with an approximate factor of 3 smaller angular velocity for the $L = 1$ state. The maximum value of the χ-angle differs for the 10 trajectories in Figure 10 and varies from 7.5−33.6° for the $L = 3$ state and 5.5−24.8° for the $L = 1$ state. With vibrational angular momentum zpe included for the 10 trajectories, χ_{max} varies from 5.4°−24.6° and 4.7°−21.3° for the $L = 3$ and 1 states, respectively. Including vibrational angular momentum zpe has the effects of increasing the period for the χ-angle motion and decreasing the value of χ_{max}.

C. Regular Versus Irregular Motion and the Effect of Anharmonicity. The plots in Figures 8−10 indicate that the classical motion is regular and not irregular (i.e., chaotic)[28] for the vibrational angular momentum states. To assess this in more detail, coordinate Fourier spectra[28,29] were calculated for trajectories with vibrational angular momentum zpe and without and with C−O stretch zpe. The diagnostic for regular dynamics is a sharp spectrum, versus a grassy spectrum for irregular dynamics.[28,29] These trajectories have regular spectra, and examples are illustrated in Figure 11. Thus, the classical motion

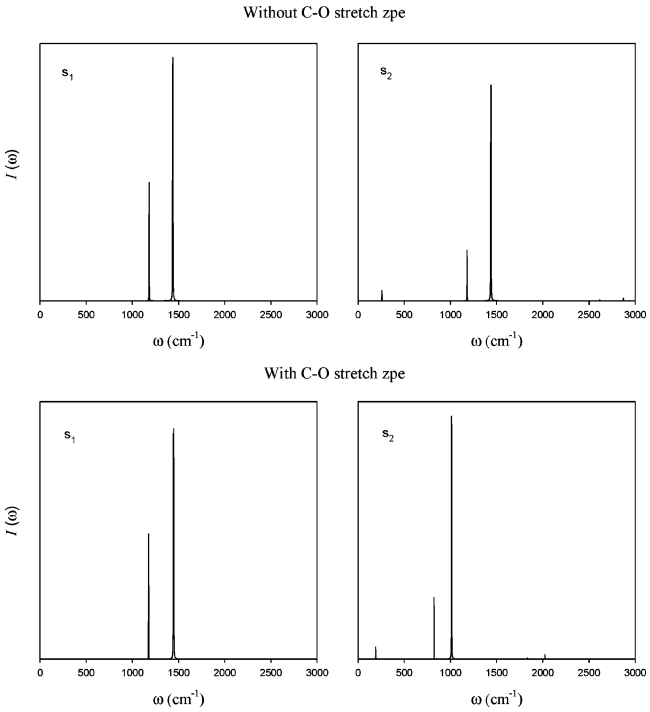

Figure 11. Coordinate Fourier spectra of a classical trajectory for the $L = N = 3$ vibrational angular momentum state, with vibrational angular momentum zpe and without (upper) and with (lower) C−O stretch zpe. Spectra are shown for the symmetric stretch, $S_1 = (\Delta r_1 + \Delta r_2)/\sqrt{2}$, and the bend, $S_2 = \Delta\theta$. The trajectories for these spectra are shown in Figures 6 and 8.

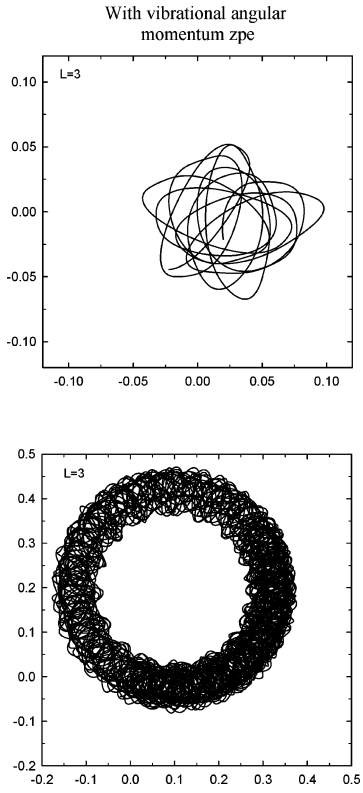

Figure 12. The same plots as in the upper-right panels of Figures 7 and 8, except a Morse function is used for the C−O stretch potential. The plot on the top is for 0.5 ps as in Figure 7, and that on the bottom is for 20 ps as in Figure 8. The trajectories include both vibrational angular momentum and C−O stretch zpe.

for the vibrational angular momentum states considered here is regular with zpe in each degree of freedom.

Differences between the CO_2 harmonic and 0−1 transition frequencies are small, and their harmonic/anharmonic ratios are 1.05, 1.03, and 1.02 for the symmetric stretch, bend, and asymmetric stretch, respectively.[30,31] These small anharmonic corrections are not expected to significantly alter the classical motion for the CO_2 zpe level. Nevertheless, to investigate any possible effects of anharmonicity, the C−O bond stretches were treated as Morse functions instead of the harmonic oscillators used for the above calculations. The dissociation energy D_e was set to 722 kJ/mol,[32,33] and this value and the force constant 15.050 mdyn/Å for the harmonic model[25] were used to determine the β_e parameter equal to $(f/2D_e)^{1/2} = 2.51$ Å^{-1}. With the inclusion of this anharmonicity, the classical motions of the vibrational angular momentum states studied here are similar to those for the harmonic model. This is illustrated in Figure 12, where the results of calculations for the $L = N = 3$ state, with both vibrational angular momentum and stretch zpe, are plotted. The plots in Figure 12 should be compared with those in the upper-right panels of Figures 7 and 8, and it is seen that the classical motions are very similar for the anharmonic and harmonic potentials.

V. Summary

In this work, an algorithm for selecting quasiclassical initial conditions for vibrational angular momentum states in chemical dynamics simulations is presented and analyzed. Applications of this algorithm are considered for initial conditions without and with zpe included in the vibrational angular momentum states and the C−O stretching modes. The O-atom motions in the *x*,*y*-plane, determined from classical trajectories in Cartesian coordinates and from the normal-mode model, are compared for the $N = 3$ and $L = 3$ and 1 vibrational angular momentum states. The inclusion of zpe in the C−O stretch modes has a significant effect on the O-atom motions for the vibrational angular momentum states. Without C−O stretch zpe, the normal-mode model predicts a fixed O−C−O angle for the $L = N = 3$ state and a circular motion in the *x*,*y*-plane, with the O−C−O equilibrium structure lying on the *z*-axis. For the $N = 3$ and $L = 1$ state, the O−C−O angle bends, and the motion is elliptical.

For the classical trajectory calculations without C−O stretch zpe, the O-atom motion for the $L = N = 3$ state without vibrational angular momentum zpe is circular and is similar to that for the normal-mode model. However, for the $L = N = 3$ state with vibrational angular momentum zpe and the two $L = 1$ states without and with vibrational angular momentum, the motion is not elliptical as it is for the normal-mode model. The short-time (i.e., 0.5 ps motion) for these latter three states is that of a rotating ellipse, whereas for long-times this ellipse rotates around the origin in the *x*,*y*-plane to form a tubular structure. The origin of the difference between the actual Cartesian O-atom motion and that predicted by the normal-mode model arises from coupling between the O−C−O bend and C−O stretch modes, including centrifugal distortion. Cartesian O-atom motions, approximating the ellipse of the normal-mode model, are obtained by using a very high force constant for the C−O stretch mode.

Including zpe in the C−O stretch modes introduces considerable complexity into the O-atom motions for the vibrational angular momentum states. In comparison to the states without C−O stretch zpe, for which there is a single trajectory for each state, the states with C−O stretch zpe do not display such a unique trajectory, because a random phase is chosen for each of the C−O stretch modes. The short-time O-atom motions for the trajectories are highly irregular and do not appear to have any identifiable characteristics. However, the O-atom motions for trajectories integrated for substantially longer periods of time acquire unique properties. Furthermore, for these longer integration times, trajectories with and without vibrational angular momentum zpe are similar, for both the $L = 3$ and $L = 1$ states, if they have the same random phases for the C−O stretch modes. The long-time O-atom motion becomes tubular for trajectories integrated to ∼14 ps for the $L = 3$ states and to ∼44 ps for the $L = 1$ states. For short integration times of 0.5 ps, an approximate time it takes two bimolecular reactants to collide, the vibrational angular momentum j_z remains aligned along the O−C−O internuclear axis. However, for longer times this is not the case, and this property is studied by determining the time dependence of the angle χ between the *z*-axis and the O−O internuclear axis. Plots of $\chi(t)$ are periodic, with a period of ∼14−16 ps for the $L = 3$ states and ∼43−49 ps for the $L = 1$ states. The maximum χ-angle in these $\chi(t)$ plots has a range of values and depends upon the random phases for the C−O stretch modes.

The algorithm used here to choose quasiclassical initial conditions for a polyatomic molecule, with degenerate bends, assumes the vibrational energy is a sum of the $(n_i + 1/2)h\nu_i$ nondegenerate bend normal-mode energies plus $(N + 1)h\nu$ for the degenerate bends. This energy only approximates the molecule's actual vibrational energy levels, because it does not include couplings between the normal modes and the dependence of the energy on the vibrational angular momentum quantum number *L*. A more accurate expression for the CO_2 energy is given by eq 21,[30,31,34,35]

$$E(\mathrm{cm}^{-1}) = \sum_{i=1}^{3}\left(n_i + \frac{d_i}{2}\right)\tilde{\nu}_i + \sum_{i=1}^{3}\sum_{j\geq i} x_{ij}\left(n_i + \frac{d_i}{2}\right)\left(n_j + \frac{d_j}{2}\right) + g_{22}L^2 \quad (21)$$

where d_i, the degeneracy of the mode, equals 2 for mode 2 and equals 1 for modes 1 and 3. It would be of interest to use this energy expression, for the quasiclassical sampling algorithm in Section III, so that this energy expression could be used to choose initial conditions for the spectroscopic energy levels. This may be done in the future.

As described above, the algorithm used here to select quasiclassical initial conditions for vibrational angular momentum states, is based on the zeroth-order normal-mode model. In future work it may be of interest to use Einstein-Brillouin-Keller (EBK) semiclassical quantization[35−44] to determine coordinates and momenta for a specific vibrational angular momentum state. For the states without C−O stretch zpe the EBK quantization will depend on the *N* and *L* quantum numbers, and this 2D quantization may be relatively straightforward. However, with C−O stretch zpe included, the quantization will also depend on the symmetric and asymmetric stretch modes, and this four-dimensional quantization will be more challenging.

Acknowledgment. This material is based upon work supported by the National Science Foundation under Grant No. 0615321 and the Robert A. Welch Foundation under Grant No. D-0005. The authors wish to thank Professor Scott Anderson for very helpful discussions and motivating this work.

References and Notes

(1) Peslherbe, G. H.; Wang, H.; Hase, W. L. In *Monte Carlo Methods in Chemical Physics, Advances in Chemical Physics,* Ferguson, D. M., Siepman, J. I., Truhlar, D. G., Eds; Wiley: New York, 1999; Vol. 105, pp 171−201.

(2) Marcus, R. A.; Coltrin, M. E. *J. Chem. Phys.* **1977**, *67*, 2609.
(3) Levine, R. D.; Bernstein, R. B. *Molecular Reaction Dynamics and Chemical Reactivity*; Oxford: New York, 1987.
(4) Swamy, K. N.; Hase, W. L. *J. Phys. Chem.* **1983**, *87*, 4715.
(5) Lu, D. -H.; Hase, W. L. *J. Chem. Phys.* **1988**, *89*, 6723.
(6) *Comparisons of Classical and Quantum Dynamics*, Advances in Classical Trajectory Methods; Hase, W. L., Ed.; JAI Press: London, 1998, Vol. 3.
(7) Wyatt, R. E.; Iung, C.; Leforestier, C. *J. Chem. Phys.* **1992**, *97*, 3477.
(8) Aoiz, F. J.; Bañares, L.; Herrero, V. J. In *Comparisons of Classical and Quantum Dynamics*, Advances in Classical Trajectory Methods; Hase, W. L., Ed.; JAI Press: London, 1998, Vol. 3, p 121.
(9) Dong, E.; Setser, D. W.; Hase, W. L.; Song, K. *J. Phys. Chem. A* **2006**, *110*, 1484.
(10) Isa, N.; Gibson, K. D.; Yan, T. -Y.; Hase, W. L.; Sibener, S. J. *J. Chem. Phys.* **2004**, *120*, 2417.
(11) Untch, A.; Schinke, R.; Cotting, R.; Huber, J. R. *J. Chem. Phys.* **1993**, *99*, 9553.
(12) Liu, J.; Uselman, B. W.; Boyle, J. M.; Anderson, S. L. *J. Chem. Phys.* **2006**, *125*, 133115.
(13) Anderson, S. L., Department of Chemistry, University of Utah, private communication, 2007.
(14) Herzberg, G. *Molecular Spectra and Molecular Structure. II. Infared and Raman Spectra of Polyatomic Molecules*; Van Nostrand Reinhold: New York, 1945; pp 75- 76.
(15) Levine, I. N. *Molecular Spectroscopy*; Wiley: New York, 1975; pp 271−277.
(16) Califano, S. *Vibrational States*; Wiley: New York, 1976; pp 37−41.
(17) Shaffer, W. H. *Rev. Mod. Phys.* **1944**, *16*, 245.
(18) Gibson, L. L.; Schatz, G. C. *J. Chem. Phys.* **1985**, *83*, 3433.
(19) Child, M. S. *Semiclassical Mechanics with Molecular Applications*; Oxford: New York, 1991.
(20) Califano, S. *Vibrational States*; Wiley: New York, 1976; p 23.
(21) Sloane, C. S.; Hase, W. L. *J. Chem. Phys.* **1977**, *66*, 1523.
(22) Bunker, D. L.; Goring-Simpson, E. A. *Faraday Discuss. Chem. Soc.* **1973**, *55*, 93.
(23) Goldstein, H. *Classical Mechanics*; Addison-Wesley: London, 1950.
(24) Hase, W. L.; Duchovic, R. J.; Hu, X.; Komornicki, A.; Lim, K. F.; Lu, D.-H.; Peslherbe, G. H.; Swamy, K. N.; Vande Linde, S. R.; Zhu, L.; Varandas, A.; Wang, H.; Wolf, R. J. *Quantum Chemistry Program Exchange Bulletin* **1996**, *16*, 671.
(25) Martínez-Núñez, E.; Rahaman, A.; Hase, W. L. *J. Phys. Chem. C.* **2007**, *111*, 354.
(26) Bunker, D. L. *J. Chem. Phys.* **1962**, *37*, 393.
(27) Reference 16, p. 278.
(28) Lichtenberg, A. J.; Lieberman, M. A. *Regular and Chaotic Dynamics*, 2nd ed.; Springer-Verlag: New York, 1991.
(29) Noid, D. W.; Koszykowski, M. L.; Marcus, R. A. *J. Chem. Phys.* **1977**, *67*, 404.
(30) Suzuki, I. *J. Mol. Spectrosc.* **1968**, *25*, 479.
(31) Chedin, A. *J. Mol. Spectrosc.* **1979**, *76*, 430.
(32) Pavlyuhko, A. I. *J. Appl. Spectrosc.* **1993**, *58*, 275.
(33) Berry, R. S.; Rice, S. A.; Ross, J. *Physical Chemistry*; Wiley: New York, 1980; p 564.
(34) Herzberg, G. *Molecular Spectra and Molecular Structure. II. Infared and Raman Spectra of Polyatomic Molecules*; Van Nostrand Reinhold: New York, 1945; p. 210.
(35) Hirst, D. M. *Potential Energy Surfaces. Molecular Structure and Reaction Dynamics*; Taylor and Francis: London, 1985; p 80.
(36) Noid, D. W.; Marcus, R. A. *J. Chem. Phys.* **1975**, *62*, 2119.
(37) Hase, W. L. *J. Phys. Chem.* **1982**, *86*, 2873.
(38) Eaker, C. W.; Schatz, G. C. *J. Chem. Phys.* **1984**, *81*, 2394.
(39) Miller, W. H. *J. Chem. Phys.* **1984**, *81*, 3573.
(40) Skodje, R. T.; Borondo, F.; Reinhardt, W. P. *J. Chem. Phys.* **1985**, *82*, 4611.
(41) Martens, C. C.; Ezra, G. S. *J. Chem. Phys.* **1985**, *83*, 2990.
(42) Grozdanov, T. P.; Saini, S.; Taylor, H. S. *Phys. Rev. A.* **1986**, *33*, 55.
(43) Duchovic, R. J.; Schatz, G. C. *J. Chem. Phys.* **1986**, *84*, 2239.
(44) Pickett, T. J.; Shirts, R. B. *J. Chem. Phys.* **1991**, *94*, 6036.